Journal of Applied Physics

Specifics of scattering and radiation from sparse and dense dielectric meta-surfaces

Cite as: J. Appl. Phys. **125**, 163106 (2019); https://doi.org/10.1063/1.5087422@jap.2019.DNM2019.issue-1
Submitted: 31 December 2018 . Accepted: 07 April 2019 . Published Online: 26 April 2019

S. Jamilan, G. Semouchkin, N. P. Gandji, and E. Semouchkina

View Online Export Citation CrossMark

ARTICLES YOU MAY BE INTERESTED IN

Journal of Applied Physics **DNM2019**, 093102 (2019); https://doi.org/10.1063/1.5078576@jap.2019.DNM2019.issue-1

Journal of Applied Physics **DNM2019**, 103106 (2019); https://doi.org/10.1063/1.5087027@jap.2019.DNM2019.issue-1

Journal of Applied Physics **DNM2019**, 133101 (2019); https://doi.org/10.1063/1.5087204@jap.2019.DNM2019.issue-1

© 2019 Author(s).

Journal of Applied Physics ARTICLE scitation.org/journal/jap

Specifics of scattering and radiation from sparse and dense dielectric meta-surfaces

Cite as: J. Appl. Phys. **125**, 163106 (2019); doi: 10.1063/1.5087422
Submitted: 31 December 2018 · Accepted: 7 April 2019 ·
Published Online: 26 April 2019

View Online Export Citation CrossMark

S. Jamilan,[1,a)] G. Semouchkin,[1] N. P. Gandji,[2] and E. Semouchkina[1]

AFFILIATIONS

[1]Department of Electrical and Computer Engineering, Michigan Technological University, Houghton, Michigan 49931, USA
[2]College of Medicine, Pennsylvania State University, Hershey, Pennsylvania 17033, USA

Note: This paper is part of the Special Topic on Dielectric Nanoresonators and Metamaterials.
[a)]**Author to whom correspondence should be addressed:** sjamilan@mtu.edu

ABSTRACT

Metasurfaces composed of nanosized silicon particles are considered prospective low-loss media for future planar devices with subwavelength thickness, capable of realizing many optical functionalities, including beam steering, focusing, and holography. Previous studies revealed an opportunity to provide directional scattering from silicon metasurfaces at Kerker's conditions and projected obtaining significantly enhanced intensity of scattering at overlapping of dipolar magnetic and electric resonances in particles at their specific geometries. Although silicon metasurfaces are usually represented by dense arrays, interactions between resonators are often neglected in their analysis, which typically uses metamaterial concepts, assuming that responses of arrays can be represented by responses of single "meta-atoms." In this work, we investigate cooperative resonance phenomena in dielectric metasurfaces, including interactions between electric and magnetic resonances within single particles and inter-resonator interactions in arrays. First, we analyze the transformation of the responses of single resonators, when their shape changes from a sphere to a cylinder, and then to a disk, and, in particular, describe the specifics of the formation of electric and magnetic dipole modes at a coincidence of resonances. Then, phenomena in arrays are considered, including the effects of arraying on resonator responses and the effects of packing density on metasurface responses. We demonstrate that dense packing causes strong changes of resonances, transverse coupling, and integration of resonance fields, affecting scattering and radiation from metasurfaces. The obtained results are important for understanding the complexity of responses of dielectric metasurfaces and provide guidance for their design and for scattering and radiation control.

Published under license by AIP Publishing. https://doi.org/10.1063/1.5087422

I. INTRODUCTION

Dielectric metasurfaces (MSs), composed of silicon nanoparticles and exhibiting essentially lower losses compared to plasmonic MSs, attract increasing attention in the development of novel photonic devices. In particular, it was demonstrated in Refs. 1–3 that scattering from MSs formed from dielectric resonators (DRs) made of silicon rods/disks could be controlled by changing the height-to-diameter ratio of the particles. Such geometric changes were shown to shift the frequencies of magnetic and electric Mie-type resonances in DRs up to their coincidence, when full transmission of incident waves through MSs was observed with 2π phase control.[3] These results were the reason for projecting that dielectric MSs will be the basic media for developing new optical devices, controlling both intensity and phases of scattered waves that is required for obtaining holographic images.[4] The observed phenomena were explained using the concepts of directional scattering from dielectric spheres at the so-called Kerker's conditions[5,6] that were thoroughly investigated in both microwave and optical ranges.[6–10] (Kerker's conditions are conditions for balancing wave flows scattered by electric and magnetic resonances in dielectric spheres leading to destructive interference of these flows in either forward or backward directions with respect to wave incidence. Realizing the 1st Kerker condition yields destructive interference of two flows in the backward direction and zero back scattering, while realizing the 2nd Kerker condition provides destructive interference in the forward direction and zero front scattering.) Similar approaches were used in the following works (for example, Ref. 11), although the physics of the observed phenomena still called for clarification. In particular, the effects of particle resonance integration in MSs were omitted from consideration in Refs. 1–3, and, instead,

Published under license by AIP Publishing.

metamaterial concepts, assuming that the response of the entire array could be represented by the response of a single "meta-atom," were used. Meanwhile, MSs investigated in Refs. 1–3 were formed from dense DR arrays, in which the interaction of particle resonance fields should be expected. In our earlier work in 2005,[12] we described such interaction and coupling phenomena, which were later observed in other works on metamaterials.[13–15] When recently conducting a set of numerical experiments[16] with the same type of arrays as those used in Ref. 3, we observed strong effects of lattice parameters on MS responses, including their forward scattering (FS) and backward scattering (BS). It was shown that at such small lattice constants as those used in Ref. 3, DRs in MSs appeared to be strongly coupled, which affected observed resonance frequencies and interaction between MSs and incident waves.

In this work, we present the results of a broader investigation aimed at a deeper understanding of various cooperative phenomena in dielectric MSs, including interactions between electric and magnetic resonances within DRs, as well as inter-resonator interactions in arrays. The obtained results are important for understanding the complexity of MS responses and provide guidance for choosing an optimal MS design. We start from the analysis of responses from single DRs placed in free space and then turn to the phenomena in arrays.

II. MODELS AND METHODOLOGY OF NUMERICAL EXPERIMENTS

"Meta-atoms" of MSs in these studies were represented by silicon DRs of various shapes [Fig. 1(a)]. The dielectric constant of DRs was 12.25 that is the typical value for silicon at optical frequencies.[17] Cylindrically shaped DRs were similar to those employed in Ref. 3; however, different from Ref. 3, the diameter of DRs was not changed to control their resonances and kept equal to 240 nm. Instead, for varying resonance frequencies, the height of DRs was changed from 240 down to 60 nm [Fig. 1(a)]. Such an approach, first used in Ref. 16, provided an opportunity for investigating the effects of lattice parameters on MS responses. Comparing the responses of DRs of different shapes allowed for observing the transformation of well-studied responses of dielectric spheres into responses of disk-shaped DRs.

Simulations were performed by using the Frequency Domain Solver of COMSOL Multiphysics and verified using the Time Domain Solver of CST Microwave Studio software packages. Plane waves, incident normally to MSs (along the Z-axis in Fig. 1), were used for excitation. To evaluate scattering from MSs, we, first, simulated S-parameter spectra, as it was done in Refs. 1–3. Such an approach suggested representing periodic DR arrays by one-cell model, conventionally used at modeling homogenized metamaterials, when one cell is assumed representing the entire medium. We employed the one-cell model with periodic boundary conditions (BCs) for calculating S-parameter spectra to characterize the interaction between MSs and incident waves. In addition, to describe radiation from resonating MSs, we employed the COMSOL technique for evaluating FS and BS spectra from finite size samples and simulated far-field patterns, thus considering MSs as sources of radiation comparable to antennas. The latter approach is often used in resonance scattering studies, which could also be referred to as resonance radiation and which is expected to play an important role in MS responses. It could be noted that at strong coupling between DRs, employment of the one-cell model requested justification. However, at weak interactions between DRs, i.e., in the cases of sparse arrays, the one-cell model was expected to provide adequate representation of array interaction with incident waves. To characterize resonance scattering/radiation from MSs, we used MS fragments consisting of 9 (3 × 3) unit cells [Fig. 1(b)], which were found to represent MSs properly, based on experiments with fragments of various sizes. Finally, to characterize resonance fields and coupling effects, we simulated field patterns in cross sections of MS fragments applying periodic boundary conditions at their boundaries.

III. ANALYSIS OF RESONANCES IN SINGLE PARTICLES AND SCATTERING FROM THEM

The upper row in Fig. 2 presents spectral changes of signals from E (electric) and H (magnetic) field probes placed either in the center (point A) of spherical and cylindrical DRs excited by plane waves or in point B near the edges of Z-directed diameters of central XZ cross sections. Signals from point A allowed for observing electric (EDRs) and magnetic dipolar resonances (MDRs),

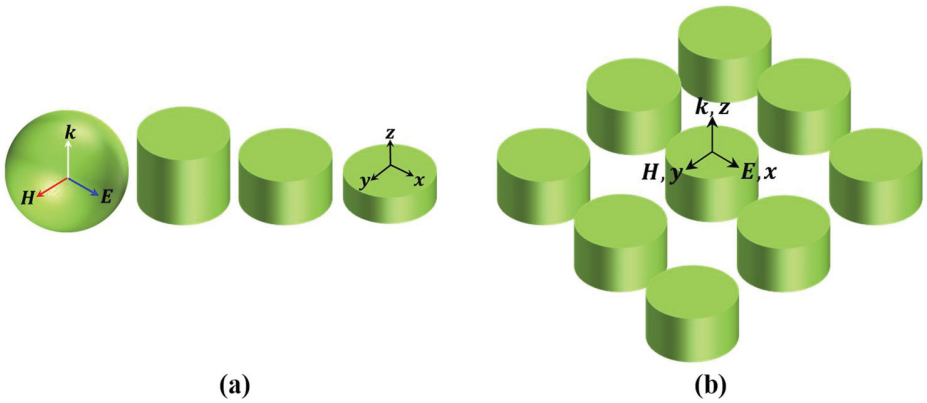

FIG. 1. Examples of (a) DRs and (b) 3 × 3 fragments of MSs used in these studies.

Published under license by AIP Publishing.

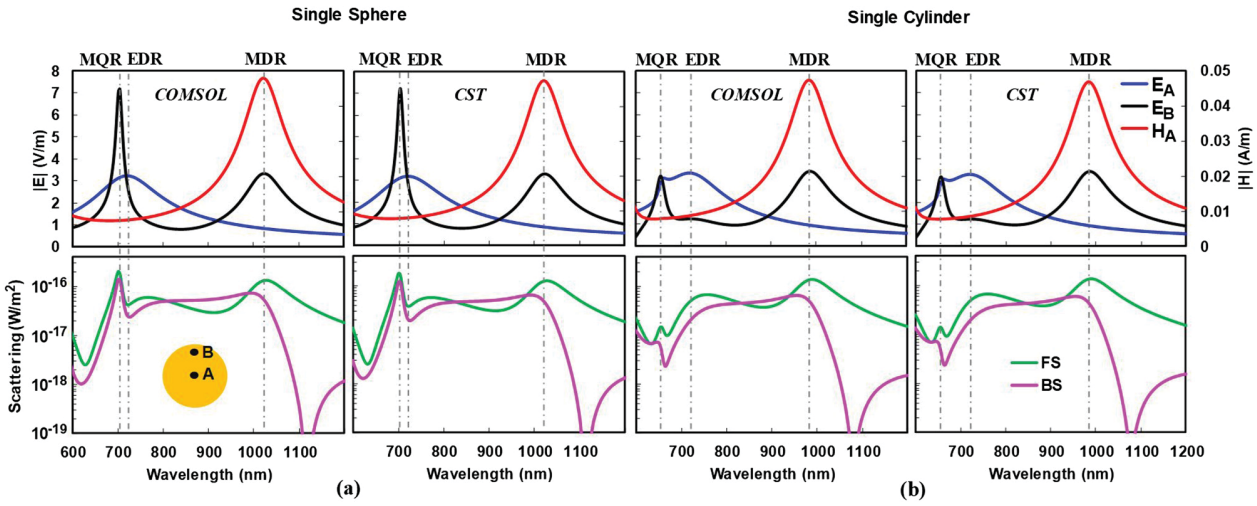

FIG. 2. Simulated using COMSOL Multiphysics and CST Microwave Studio packages spectra of signals from E- and H-field probes placed in point A and from E-field probes placed in point B (upper row) and spectra of BS and FS power density (lower row) for DRs with (a) spherical and (b) cylindrical shapes. The inset shows positions of field probes in the central XZ cross section of DRs. Diameter of spheres is 278 nm, while cylindrical DRs have both diameter and height equal to 240 nm.

while signals from point B were characterizing magnetic quadrupolar resonances (MQR) formed at the blue tails of EDRs. Diameters of spherical DRs were slightly increased compared to diameters of cylindrical DRs to provide in two types of DRs similar frequencies of EDRs and MDRs. As seen in the graphs, while the strengths of dipolar resonances in two DRs are comparable, MQR in spheres is twice stronger than that in cylindrical DRs, and f_{MQR} for spheres is closer to f_{EDR}. In general, however, the spectra of responses from two DR types, as well as their BS and FS spectra, given in the lower row of Fig. 2, demonstrate similar features at $f < f_{EDR}$ ($\lambda > \lambda_{EDR}$) and do not reveal any differences by employing various software in simulations.

The spectra of BS and FS for two types of DRs demonstrate higher BS compared to FS in the range between EDRs and MDRs that is the characteristic for the 2nd Kerker condition and show deep drops of BS (at seemingly undisturbed FS) at $f < f_{MDR}$ ($\lambda > \lambda_{MDR}$) that is typical for the 1st Kerker condition. Such similarity confirms that dipolar resonances in cylindrical DRs with heights close to their diameters are analogous to Mie resonances in spheres. The difference in BS and FS spectra of two DRs at $f > f_{EDR}$ ($\lambda < \lambda_{EDR}$) appears due to differences in MQR responses.

Figure 3 presents spectral distributions of BS [Fig. 3(a)] and FS [Fig. 3(b)] power density, provided by single cylindrical DRs of different heights at their excitation by incident plane waves. The positions of EDR and MDR, obtained from the spectra of signals from E- and H-field probes placed in DR centers, are marked in the presented patterns by white and black circles, respectively. It is seen in the figures that the curves, representing EDRs and MDRs, cross each other at DR heights close to 90 nm that is in agreement with the data in Refs. 1–3. However, these crossings are not

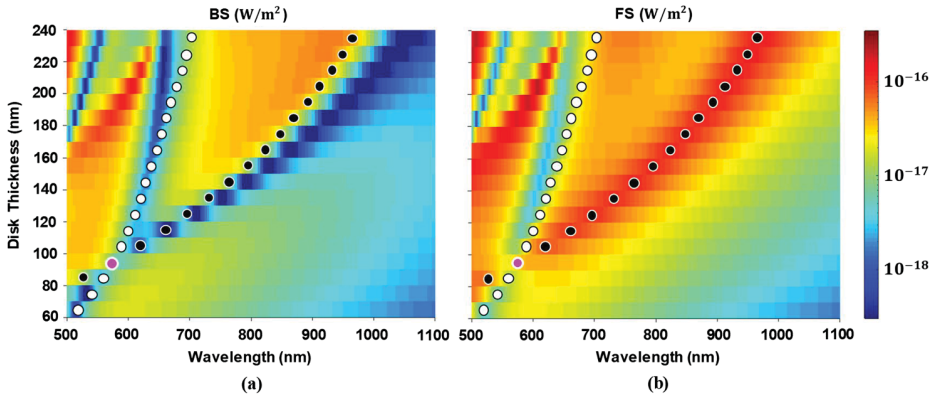

FIG. 3. Spectral distributions of (a) BS and (b) FS for single cylindrical DRs of various heights at occurrence of EDRs, MDRs, and MQRs. Diameters of DRs are equal to 240 nm. White and black colored circles mark spectral positions of EDRs and MDRs. Purple circles on two graphs mark the case, when frequencies of EDR and MDR coincide.

Published under license by AIP Publishing.

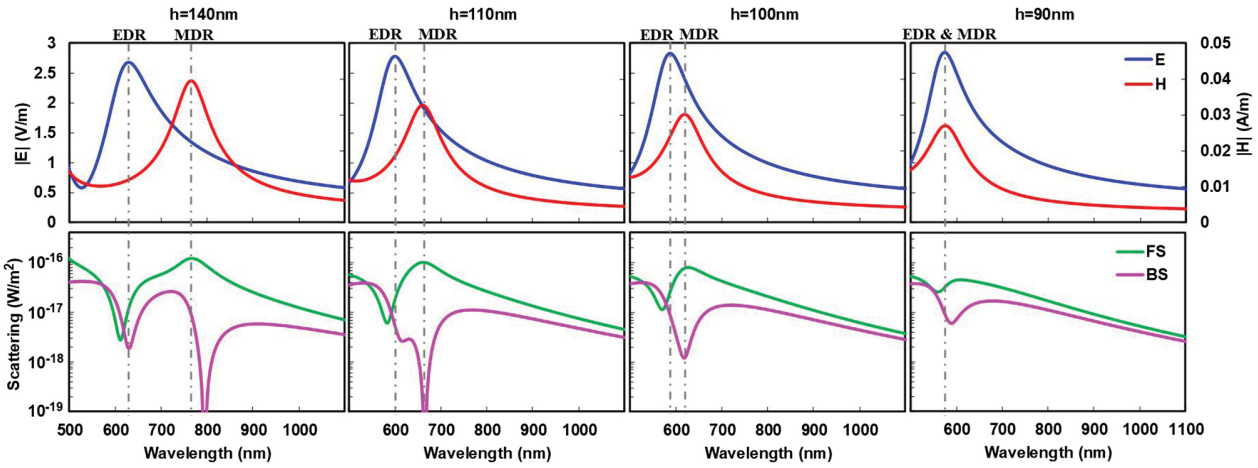

FIG. 4. Upper row: spectra of signals from E- and H-field probes placed in centers of DRs with heights from 140 down to 90 nm. Lower row: respective BS/FS spectra. Disk heights are indicated above the columns.

accompanied either by increase of FS or BS or by deep drops of these values, which would allow one to detect specific directional scattering from MSs composed of 90 nm height DRs. It is well observed that, while MDRs provide strong and wideband FS, which gradually decreases at smaller DR heights, EDRs produce comparable FS only at DR heights close to 240 nm, while at heights below 210 nm, FS, caused by EDRs, drops down by an order of magnitude and more. BS at EDRs also looks significantly weaker than BS at MDRs at DR heights, starting from 240 nm down to, at least, 140 nm. It is worth noting here that meaningful FS and BS can be seen at MQRs, visualized at higher frequency sides of the blue colored "canyons" adjusting to the curves of EDRs. A deeper and wider "canyon" is seen in the BS pattern to the right of the curve of MDRs. It seems related to realizing the 1st Kerker condition (see Fig. 2), i.e., conditions for destructive interference of waves scattered by EDR and MDR in the backward direction. It is important to mention that the tails of two "canyons" in the BS pattern come closer to each other at DR heights of about 110 nm, when a strong FS provided by MDR still exists. It shows an opportunity for obtaining directional scattering at MDR frequencies.

Figure 4 shows changes of resonance responses and BS/FS spectra for single cylindrical DRs at decreasing their heights from 140 down to 90 nm (to the case when frequencies of EDR and MDR coincide). It can be seen that at the DR height of 140 nm, when EDR and MDR are still relatively far from each other, they affect BS/FS spectra differently. At EDR, both BS and FS drop down, demonstrating the same trend as could be noticed for spheres in Fig. 2, while at MDR, when FS, as in the case of spheres, remains high, BS experiences a wideband descend, approaching a deep drop below 10^{-19} W/m^2, which is defined by realizing the 1st Kerker condition.

At the smaller DR height of h = 110 nm, Kerker's condition gets realized exactly at the frequency of MDR. It is worth mentioning that the observed effect looks accompanied by the decrease of MDR strength. With a further decrease of DR height down to 100 nm, the BS/FS drops lose their depths in the vicinity of EDR and Kerker's effect also decreases, although EDR and MDR frequencies still remain different. At h = 90 nm, when EDR and MDR coincide, all features of BS/FS spectra, specific for resonances, continue to degenerate so that considering the observed scattering as a clearly directional phenomenon, defined by Kerker's effect, loses any sense.

To understand the reasons, which cause deterioration of scattering capabilities of disk resonators at decreasing their heights, we have simulated field distributions in disk cross sections at EDR and MDR in DRs of various heights. It could be inferred that in disk DRs of small heights, excitation of competing resonances could be incapable of forming authentic dipoles. Figure 5 presents the data confirming significant distortions of resonance modes, when EDR and MDR frequencies approach each other. While at h = 150 nm field patterns at both resonances still look corresponding to typical images of electric and magnetic dipoles directed along the normal to each other diameters of cylindrical DR, at a DR height of 100 nm, we observe shifting of the location of the electric dipole center along the Z-axis and curving of H-field lines around the shifted position of the electric dipole center. At h = 90 nm, the above trends become enhanced so that electric dipole starts to look as formed near the upper disk surface, while magnetic dipole—as represented by an arc of a circle. Such transformations of the resonance modes could be responsible for distortions described above in the spectra of BS and FS from disk resonators.

IV. EFFECTS OF DR ARRAYING ON BS/FS AND S21 SPECTRA OF MS FRAGMENTS

As we have shown earlier in Ref. 16, DR arraying could seriously affect MS responses and cause changing of their resonance frequencies and scattering parameter spectra. According to Ref. 16, such small lattice constants, as those used in Refs. 1–3, i.e., of 330 nm, made resonance fields of cylindrical DRs with diameters of 240 nm strongly coupled so that complicated gridlike field patterns incorporating both dipole fields inside DRs and the fields in gaps

Published under license by AIP Publishing.

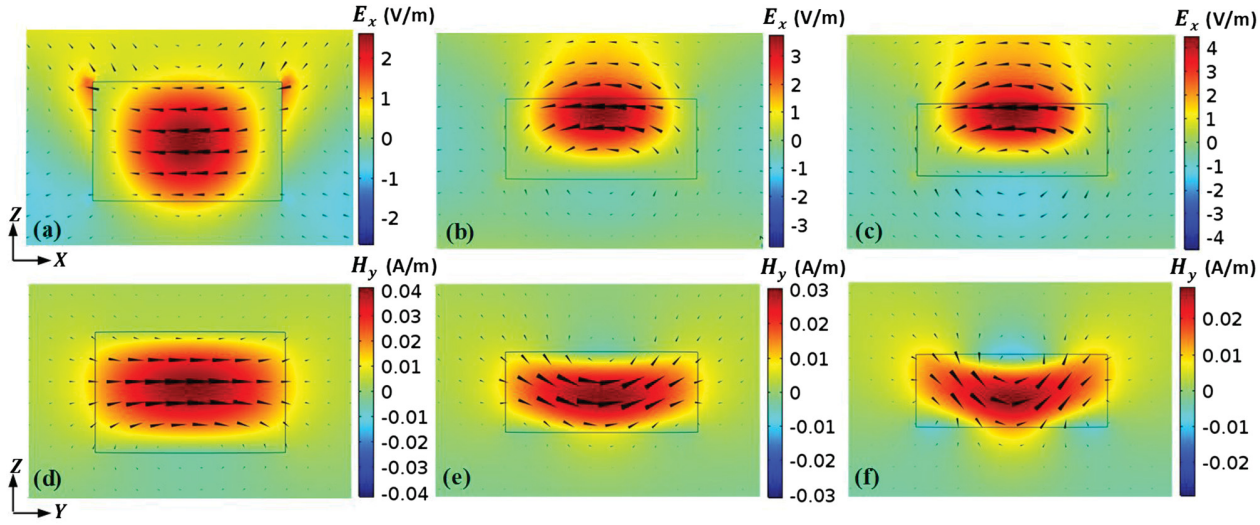

FIG. 5. Upper row—E-field patterns in XZ cross section of DRs at EDRs: (a) λ = 638 nm, h = 150 nm, (b) λ = 588 nm, h = 100 nm, and (c) λ = 574 nm, h = 90 nm. Lower row—H-field patterns in ZY cross section at MDRs: (d) λ = 793 nm, h = 150 nm, (e) λ = 619 nm, h = 100 nm, and (f) λ = 574 nm, h = 90 nm.

between resonators became seen in planar cross sections of MS. These data imply that responses of dense MS could not be considered as the sum of responses from independent DRs and that effects of integration of elementary responses in MS media should be accounted for. However, in this section, we first analyze relatively soft resonance integration in MSs, expected, according to Ref. 16, at an array lattice constant of 450 nm, and then, in Sec. V, switch to the analysis of cases with significant integration of resonances.

Figure 6 presents spectral distributions of BS and FS power density provided by 3 × 3 fragments of MSs composed of cylindrical DRs of various heights. From comparison with Fig. 3 for single resonators, it is seen that the basic features of respective distributions are quite comparable. However, there are also some differences between distributions in Figs. 3 and 6, i.e., lower frequencies of EDRs and higher frequencies of MDRs, higher BS at both EDR and MDR, and also higher FS at EDR. It is also worth mentioning that curves marking resonances in Fig. 6 have crossings at larger DR height and at higher wavelength compared to crossings in Fig. 3. In addition, Fig. 6 demonstrates relatively high BS intensities in the spectral regions between EDR and MDR, and low FS intensities in these regions. These specific features are characteristic for realizing Kerker's conditions of the 2nd type and, correspondingly, for directional scattering with dominant backward radiation [as confirmed later in Fig. 8(a)]. The presented data show that DR arraying provides a wide bandwidth for this phenomenon. It is also worth noting the differences in appearances of "canyons" with suppressed BS at $f < f_{MDR}$ ($\lambda > \lambda_{MDR}$) and at $f > f_{EDR}$ ($\lambda < \lambda_{EDR}$), and with suppressed FS at $f > f_{EDR}$ ($\lambda < \lambda_{EDR}$) in Figs. 3 and 6, although it is difficult to qualitatively describe these differences, since the scales of power density in two figures differ by about two orders of magnitude.

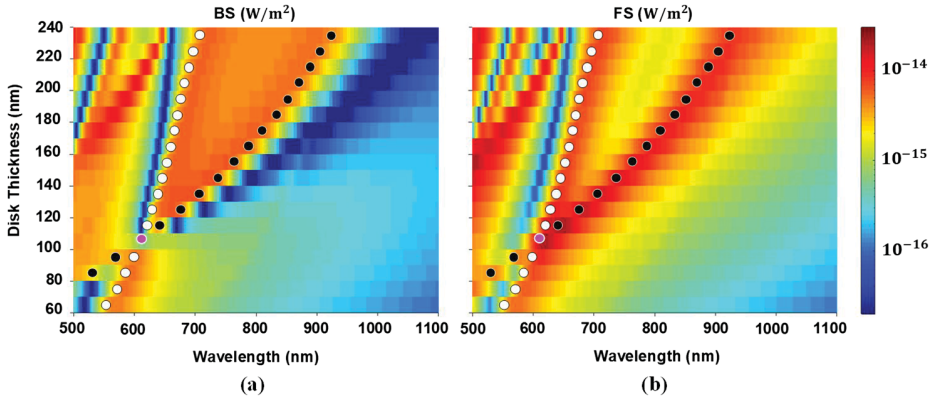

FIG. 6. Spectra distributions of BS and FS power density for 3 × 3 fragments of MSs composed of cylindrical DRs with heights ranging from 240 to 60 nm. Diameters of DRs are equal to 240 nm, lattice constants of MSs are 450 nm. Spectral positions of EDRs and MDRs are marked, respectively, by white and black colored circles. Purple circles on two graphs mark the case, when frequencies of EDR and MDR coincide.

Published under license by AIP Publishing.

Figure 7 presents spectral distributions of signals from E- and H-field probes placed in DRs to control resonances in MSs, scattering parameter spectra calculated for infinite MSs, and spectral distributions of BS and FS power density characteristic for 3 × 3 fragments of the same MSs. All data were obtained for MSs composed of DRs with the heights chosen within the range from 240 down to 100 nm.

As seen in Fig. 7, at h = 240 nm, i.e., when DR responses are comparable to responses of spheres, EDR frequency for the array is

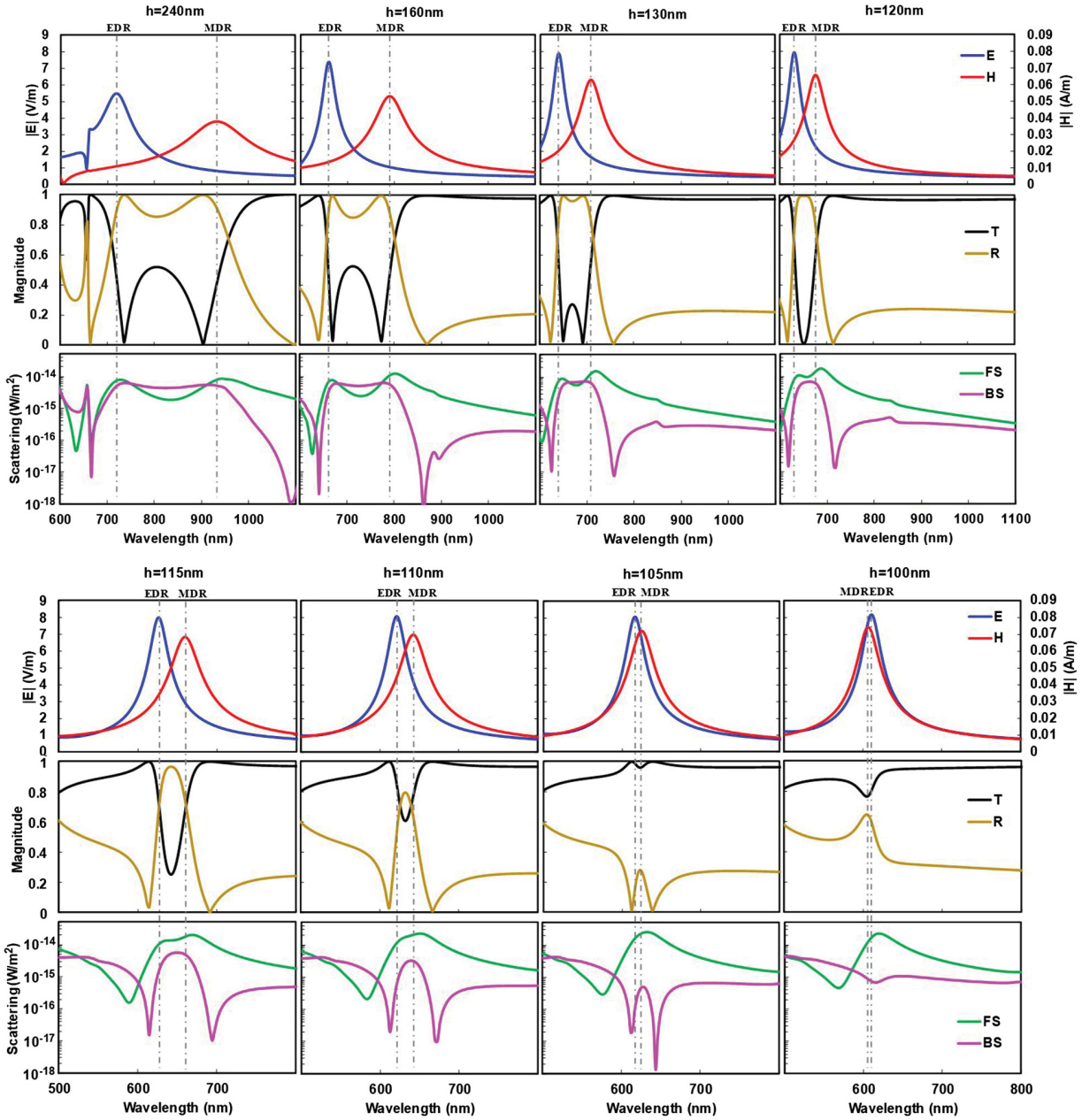

FIG. 7. Spectral distributions of electromagnetic (EM) responses from MSs differ by DR heights (shown above each column). Upper group of data—for h: 240, 160, 130, and 120 nm. Lower group of data—for h: 115, 110, 105, and 100 nm. Upper row in both groups: signals from E- and H-field probes in the centers of DRs at modeling MSs by single cells with periodic boundary conditions; middle row: S-parameters (|S21| = T and |S11| = R) simulated at above conditions; lower row: BS and FS spectra for 3 × 3 fragments of MSs.

Published under license by AIP Publishing.

close to the EDR frequency for single resonators [Fig. 2(b)], while MDR frequency for the array appears to be higher than that for single DR [Fig. 2(b)]. EDR in the array looks stronger, while MDR—weaker than in the case of single resonators—and Q-factors of resonances in the array seem to be a little higher than those in the case of a single DR. All these changes are expected to happen at arraying, which, in fact, should slightly decrease the space for forming the field "halos" of DR resonances. It could be noted that MQR is not distinctly seen in the spectra presented in Fig. 7, in contrast to the case of single DR; however, despite this, MQR still seems to be located at the same frequency (i.e., at $\lambda = 650$ nm), since field patterns in DR cross sections (not presented here) confirm characteristic for MQR field distributions just at this frequency. MQR also appears to be responsible for the specific changes observed in the scattering parameter spectra and in the BS/FS spectra at $f > f_{EDR}$. In the S-parameter spectra, while moving from EDR to MQR, we see, first, a deep drop of S11, while S21 approaches the maximum value of "1." Then, at f_{MQR}, S21 drops down, while S11 forms a peak. The values of both BS and FS drop down closer to MQR but then also form peaks at $f = f_{MQR}$.

At frequencies below f_{EDR} ($\lambda > \lambda_{EDR}$), the S21 spectrum demonstrates clear dips at frequencies close to f_{EDR} and f_{MDR}. Such dips are often considered as a proof of resonances, which are expected to cause total reflection and no transmission for incident waves. However, it is seen from Fig. 7 that at the resonance frequencies, the values of S21 and S11 appear equal. It means that the energy scattered in the forward direction becomes equal to the energy scattered in the backward direction that is characteristic, in particular, for the bagel-type radiation patterns. Described features are clearly seen at decreasing DR heights in MSs down to 120 nm, and even to 110 nm when, instead of two overlapped S21 dips, one dip is observed, which is decreasing at decreasing DR heights. It is worth noting here, however, that FS spectra do not demonstrate any dips or drops and look comparable to spectra representing the power radiated by single particles at resonances (see Fig. 2). In contrary to FS, deep drops observed in BS spectra of MS fragments appear well correlated with drops in the spectra of S11. As seen in Fig. 7, this correlation is conserved at the heights of DRs ranging from 240 down to 105 nm, and only at the height of about 100 nm, when frequencies of EDR and MDR coincide, it disappears because of degradation of all features of the spectra. At small DR heights, the frequencies of BS and S11 drops at $f > f_{EDR}$ ($\lambda < \lambda_{EDR}$) tend to become very close to f_{EDR}, while FS drops get increasingly separated from BS drops and shifted to higher frequencies (shorter λ). BS drops, which are observed at $f < f_{MDR}$ ($\lambda > \lambda_{MDR}$) in spectra of all MSs with DR heights ranging from 240 down to 105 nm, could be, without a doubt, related to realizing Kerker's conditions of the 1st type as in the single resonators. In MSs with smaller DR heights, the frequencies, at which these drops occur, get significantly higher, i.e., they shift following f_{MDR} to approach f_{EDR}. To additionally verify the relation of BS drops at $f < f_{MDR}$ to Kerker's conditions, we simulated far-field patterns provided by radiation from MS fragments at the frequencies of interest. Figure 8(b) shows that the latter BS drops mark the formation of far-fields corresponding to directional FS expected at Kerker's conditions. Common features of BS and S11 drops at $f < f_{MDR}$ and at $f > f_{EDR}$ allow for suggesting that the latter drops are also defined by realizing conditions similar to Kerker's conditions of the 1st type. In principle, approaching these conditions at $f > f_{EDR}$ could be expected, since phase jumps of dipole field oscillations at EDR and MDR should make the relation between phases of oscillations in high-frequency tails of EDR and MDR close to the relation characteristic for $f < f_{MDR}$. Far-field patterns characterizing radiation from MS fragments at frequencies corresponding to drops in BS and S11 at $f > f_{EDR}$ [Fig. 8(c)] confirm obtaining at these frequencies clearly expressed directional FS, typical for the 1st Kerker conditions.

The features of S11 and BS/FS spectra of MSs at heights of DRs providing coincidence of EDR and MDR frequencies need additional comments. It is well observed from Fig. 7 that this coincidence leads to degradation of characteristic features of both BS and FS spectra, i.e., no deep drops can be seen any more and,

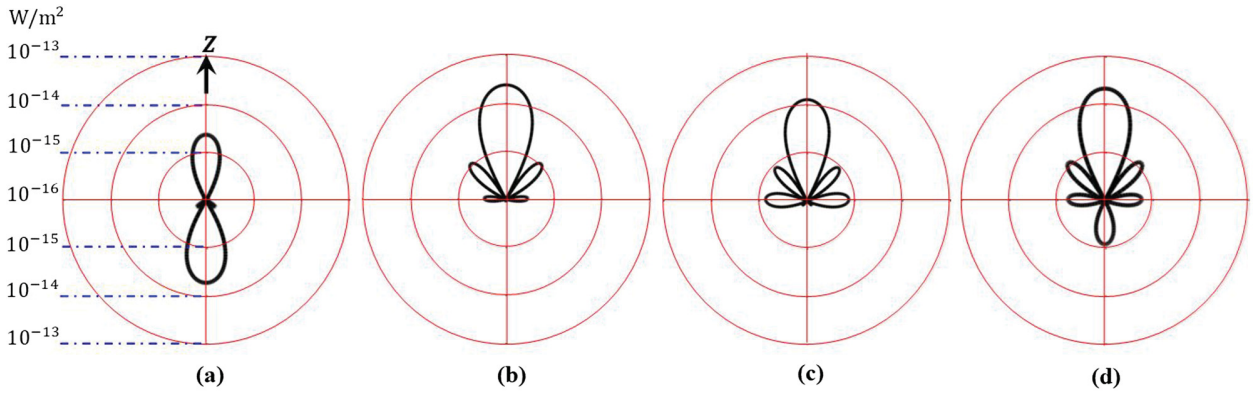

FIG. 8. Far-field patterns representing radiation from fragments of MSs: (a) at $f_{EDR} > f > f_{MDR}$, for DR heights within 120 nm < h < 240 nm, when realizing Kerker's condition of the 2nd type is expected (exemplified at h = 160 nm at $\lambda = 731$ nm); (b) at BS drops observed at $f < f_{MDR}$, when realizing 1st Kerker's condition is expected (exemplified at h = 105 nm at $\lambda = 643$ nm); (c) at BS drops observed near f_{EDR} for smaller DR heights (exemplified at h = 105 nm at $\lambda = 612$ nm); (d) at EDR and MDR approaching coincidence, when DR height is of about 100 nm (exemplified at h = 100 nm at $\lambda = 624$ nm). Black arrow shows the direction of wave incidence.

Published under license by AIP Publishing.

therefore, a discussion about realizing Kerker's conditions either at $f < f_{MDR}$ or at $f > f_{EDR}$ loses sense. BS intensity increases all over the spectrum, approaching FS intensity. This does not allow for obtaining desirable directivity of scattering [Fig. 8(d)]. It is interesting to note that, different from the data in Refs. 1–3, our data show a drop of S21 at weak peaking of S11 at the common resonance frequency of EDR and MDR. This also shows that coincidence of EDR and MDR does not provide an optimal solution for obtaining unidirectional scattering, while a much better result can be achieved by employing MSs with DRs of larger heights providing close but distant positions of dipolar resonances in the spectrum.

Finally, it is worth pointing out that the observed correlation between BS spectra of 3×3 fragments of MSs and S11 spectra, obtained for unit cells with periodic boundary conditions, i.e., for infinite MSs, confirms that at a lattice parameter of 450 nm, single unit cells of MSs are still capable of representing MS responses adequately. This also confirms that 3×3 fragments of MSs with a lattice constant of 450 nm can be used to represent radiation capabilities of the entire MSs.

V. EFFECTS OF LATTICE CONSTANT DECREASE ON BS/FS AND S21 SPECTRA OF MS FRAGMENTS

In this section, the responses of MSs with essentially smaller lattice constants of 300 nm are investigated for comparison with the results presented in Sec. IV. At such small lattice constants, we earlier observed significant changes in MS performance,[16] pointing out at the formation of integrated responses of the media, different from the responses of single particles. Figure 9 presents spectral distributions of BS and FS power densities provided by 3×3 fragments of MSs composed of cylindrical DRs of various heights. From the comparison of Fig. 9 with Fig. 6, obtained for MSs with lattice constants of 450 nm, it is seen that, although decreasing the lattice constant down to 300 nm does not eliminate main features of spectral distributions of BS and FS, essential changes of these distributions are obvious. First, total decrease of BS power density in the area between EDR and MDR, especially at smaller DR heights, can be observed. FS power density is also decreased, but not so strongly. In addition, FS power density becomes more uniformly distributed in the region between EDR and MDR, so that no so significant FS decrease in the central part of this region, comparable to the decrease seen in Fig. 6, is registered. At a total decrease of BS power, it seems that Kerker's conditions of the 2nd type could not be realized in densely packed MSs. One more visible change is blueshifts of EDR positions in the spectra. Similar EDR shifts at decreasing MSs' lattice constants were noticed in Ref. 16. As a result of this shifting, the curve of white circles marking EDRs in the BS pattern looks coinciding with the curve marking maximal canyon depths. Shifting of EDR frequencies also places the curve of white circles, connecting EDR markers, in touch with the "canyon" observed in the FS pattern, while at lattice constants of 450 nm, a similar curve was located at a relatively significant distance from the "canyon."

This happens since the spectral position of the "canyon" in the FS pattern is more stable with respect to lattice constant changes, than spectral positions of EDRs. It follows from the data, presented in Fig. 9, that in dense MSs, EDRs are not able to support strong FS power, as they do in more sparse MSs (Fig. 6). Considering MDRs, it can be noticed that, for MSs with lattice constants of 300 nm, the curves of black circles, marking MDRs in the BS/FS patterns in Fig. 9, have less steep slopes than those in Fig. 6. This means that MDR frequencies also experience blueshifts, which become bigger at smaller DR heights, although still remain smaller than EDR shifts. It is worth noting that, as the result of different characters of EDR and MDR shifting at decreasing the lattice constants, the crossing of the curves, connecting EDR and MDR markers, appears at approximately the same frequency and at approximately the same DR height for arrays with large (450 nm) and small (300 nm) lattice constants.

Figure 10 presents spectral distributions of signals from E- and H-field probes placed in DRs to control resonances in MSs, scattering parameters spectra calculated for infinite MSs using one-cell model with periodic boundary conditions, and spectral distributions of BS and FS power density characteristic for 3×3 fragments of the same MSs. The data presented in Fig. 10 were obtained, as in Sec. IV, for MSs composed of DRs with the heights chosen within the range from 240 down to 100 nm. As seen in the figure, at h = 240 nm, MQR demonstrates Fano-type shape of its resonance curve and is located in the spectrum much closer to EDR, compared to the case of MSs with a lattice constant of 450 nm. The

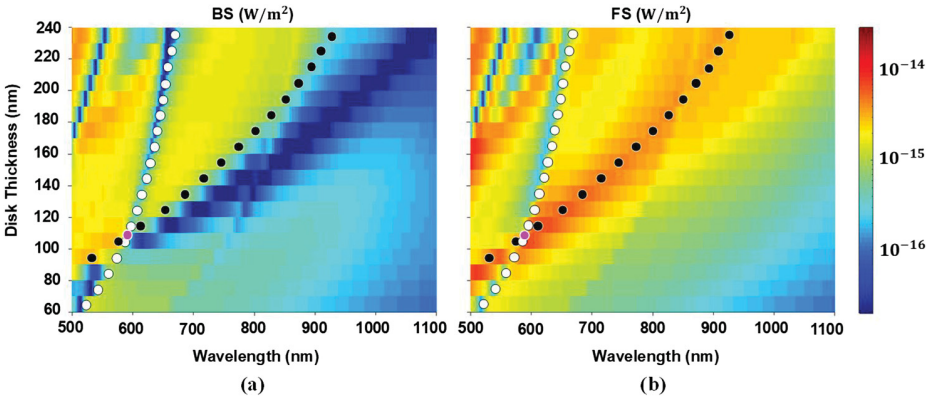

FIG. 9. Spectral distributions of BS and FS power densities for 3×3 fragments of MSs composed of DRs with heights ranging from 240 nm to 60 nm. Lattice constants of MSs are 300 nm; diameters of DRs are equal to 240 nm. Spectral positions of EDRs and MDRs are marked, respectively, by white and black colored circles. Purple circles on two graphs mark the case, when frequencies of EDR and MDR coincide.

Published under license by AIP Publishing.

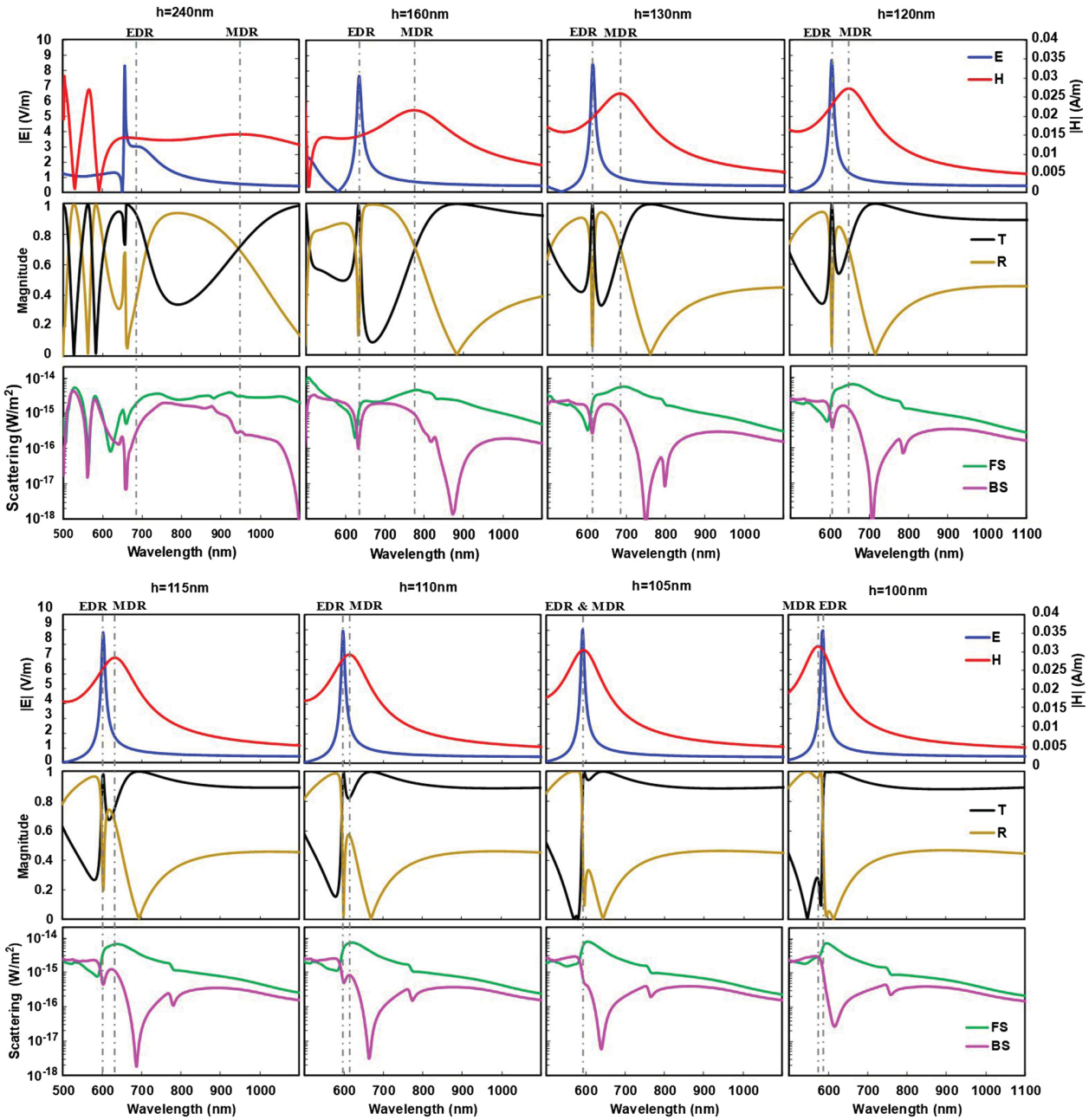

FIG. 10. Spectral distributions of EM responses from MSs, which differ by DR heights (shown above every column). Upper group of data—for h: 240, 160, 130, and 120 nm. Lower group of data—for h: 115, 110, 105, and 100 nm. Upper row in both groups: signals from E- and H-field probes located in the centers of DRs at modeling MSs by single cells with periodic boundary conditions; middle row: S-parameters simulated at above conditions; lower row: BS and FS spectra for 3 × 3 fragments of MSs.

characteristic for Fano-type resonances drops of E-field probe signals down to zero on the higher frequency sides of EDRs continues to be seen at decreasing DR heights down to 120 nm; however, at this decrease, they shift further away from EDR to the blue side of the spectrum. Considering the difference between S-parameters spectra for MSs with DR heights of 240 and 160 nm and also the difference in BS/FS spectra of respective MSs at $f > f_{EDR}$, it can be concluded that at h = 160 nm, the MQR related effects leave the EDR vicinity.

Published under license by AIP Publishing.

However, a new phenomenon appears instead: a narrowband drop of the reflection coefficient S11 down to almost zero accompanied by sharp peaking of S21 parameter up to 1 exactly at EDR frequencies. At a first glance, the new phenomenon could be compared to the scattering described in Sec. IV in sparse MSs at $f > f_{EDR}$, which we found to be similar to the effects observed at the 1st Kerker condition, with typical deep drops of BS at a relatively high FS. However, the phenomena in sparse MSs were always observed at $f > f_{EDR}$ and not at $f = f_{EDR}$. In addition, they were not narrowband and, instead of peaks of transmission, demonstrated relatively high transmission in a wide band. Therefore, the new phenomenon with delta-function-like changes in scattering parameters spectra at $f = f_{EDR}$, particularly in MSs with h = 120 and 130 nm, resemble, rather, electromagnetically induced transparency (EIT). Taking into account observations of Fano resonances in MSs, which, as known, are related to interference processes, realization of EIT in dense MSs could be expected, even though additional studies should be conducted for clarifying the underlying physics. In any case, it is not excluded that just EIT was responsible for the full transmission observed in Ref. 3 though MSs at EDR and MDR coincidence.

Different from EDRs, MDRs in dense MSs do not show new specifics, neither in S11/S21 spectra nor in BS/FS spectra, compared

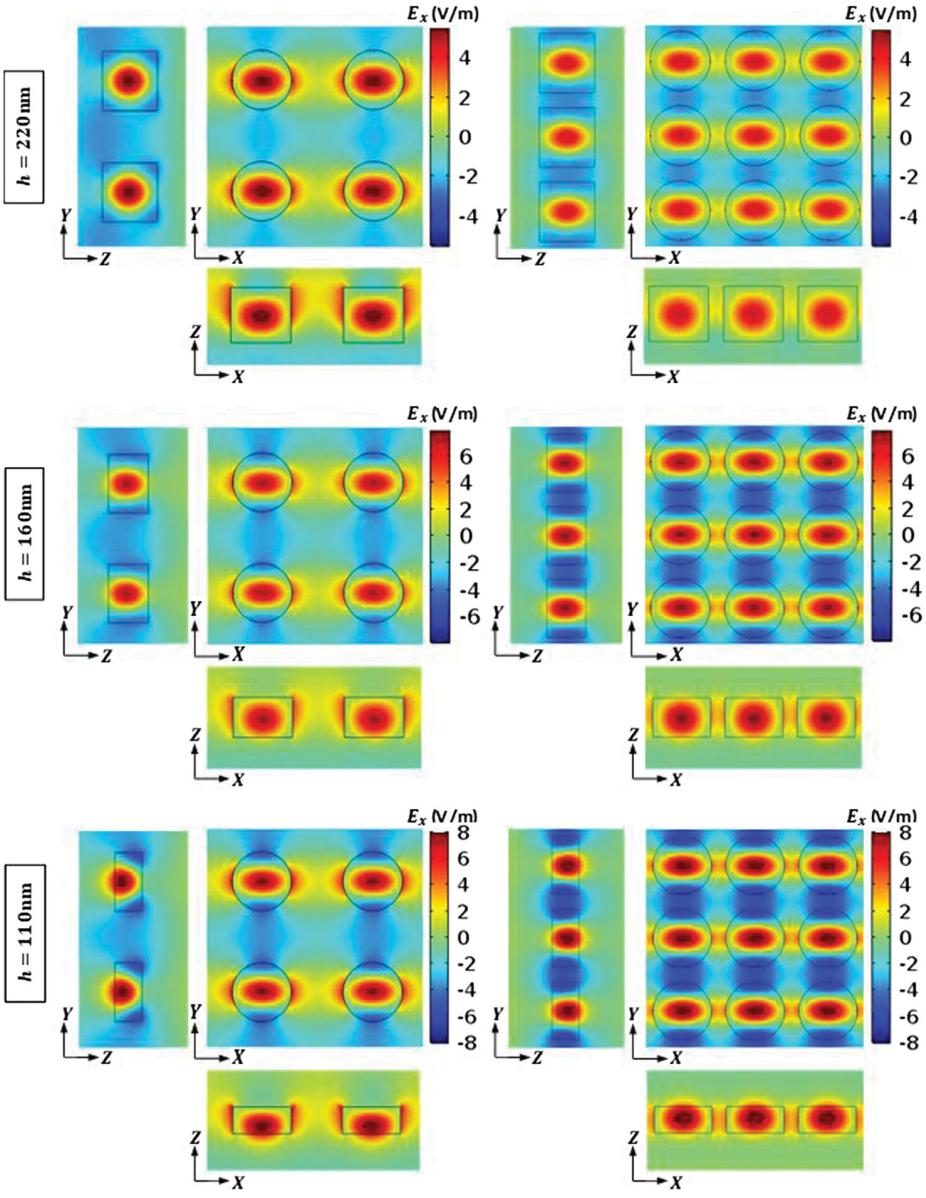

FIG. 11. Distributions of E-fields in XY, YZ, and XZ central cross sections of MSs composed of DRs with heights: 1st row—h = 220 nm; 2nd row—h = 160 nm; 3rd row—h = 110 nm with the lattice constants of 450 nm (left column) and 300 nm (right column). All patterns are obtained at the frequencies of EDRs.

Published under license by AIP Publishing.

to MDRs in sparse MSs, except for the coincidence of MDR frequencies with frequencies, at which S-parameter spectra demonstrate crossings of S11 and S21 spectra. It is seen from Fig. 10 that, different from the data for sparse MSs, S-parameter spectra of dense MSs do not show deep drops of S21, demonstrating just decreased S21 values at frequencies $f_{EDR} > f > f_{MDR}$. In contrast, S11 values increase in this frequency range, particularly at DR heights exceeding 120 nm. At smaller DR heights, the decrease of S21 and the increase of S11 look gradually degrading because of narrowing the gap between EDR and MDR owing to the fact that the blueshifts of MDRs exceed the blueshifts of EDRs. Different from MSs with a lattice parameter of 450 nm, approaching the coincidence of MDR and EDR frequencies is not accompanied by the disappearance of BS drop caused by realizing Kerker's conditions. As seen in the columns of Fig. 10 for two smallest DR heights, BS drops continue to be well observed in BS/FS spectra as at coincidence of resonances, so even at reversing positions of EDR and MDR in the spectra. It is worth mentioning here that FS increases at decreasing DR heights; however, the peak values of this radiation are observed at frequencies slightly exceeding the resonance frequencies. According to the results presented in Fig. 10, better directionality of scattering should be observed not at the common for EDR and MDR resonance frequency of 600 nm but at the frequency, which provides the realization of Kerker's condition (640 nm).

To understand the reasons, defining changes of MS responses at decreasing the array packing density, we simulated field patterns in cross sections of MSs with different lattice constants and with different DR heights. Figure 11 presents the respective distributions for electric fields.

As seen in the figure, all MSs under study have demonstrated, in their central XY cross sections, gridlike field distributions characteristic for coupled DR arrays.[18] The lines of grids are defined by X and Y axes passing through the centers of DRs. Grid lines, going along the X-axis, seem to be formed by extensions of resonance fields, which accompany the formation of electric dipoles in the centers of DRs. The fields in these extensions on two sides of each X-oriented gap between DRs look co-directed with dipoles and demonstrate the trend for overlapping. The sequences of Y-oriented gaps seem forming Y-directed lines of the grid. In Y-oriented gaps, electric fields appear directed oppositely to dipoles inside DRs. These fields can be considered as originating from electric field lines circling around neighboring resonating dipoles and overlapping within the gaps. In narrow gaps, specific for MSs with a lattice constant of 300 nm (dense MSs), fields in the gaps become enhanced up to the level of fields inside DRs. The strength of gap fields also increases with decreasing the DR heights in MSs; however, this effect is much weaker than the effect of decreasing the lattice constant. The observed enhancement of gap fields in MSs with a lattice constant of 300 nm at $h < 160$ nm allows for considering Y-sides of field grids as chains of oppositely directed dipoles. It is not excluded that such transformation of field patterns in dense MSs makes reflection from MSs at $f = f_{EDR}$ negligible and causes characteristic for them EIT-type full transmission at frequencies of EDRs. The grids with alternating resonance fields could also be the reason for the observed degeneration of BS drops at $f = f_{EDR}$ in spectra of MSs with a lattice constant of 300 nm (Fig. 10) at decreasing DR heights. By analyzing comparable BS drops observed in spectra of MSs with a lattice constant of 450 nm at $f > f_{EDR}$ (see Sec. IV), we assumed that they could be related to another realization of Kerker's conditions of the 1st type for interference of radiation from two dipolar resonances. Alternatively oriented dipoles could affect the realization of these conditions in MSs with a lattice constant of 300 nm, due to destructive interference of radiation from dipoles and resonance fields in Y-gaps.

One more interesting effect can be seen when comparing field distributions for MSs with lattice constants of 450 and 300 nm at $h = 110$ nm. In the YZ cross section of MS with a lattice constant of 450 nm, it is well observed that the centers of electric dipoles are shifted relatively to the centers of DRs, similar to that observed in Fig. 5 for single DRs. Meanwhile, in MS with a lattice constant of 300 nm, no similar shifting is detected, apparently, due to decreased freedom of resonance formation in MSs with closely packed neighboring resonators.

VI. CONCLUSION

We have investigated the directivity and power density of radiation from MSs composed of cylindrical silicon resonators, organized in square lattices, with sparse and dense packing, in spectral ranges involving magnetic and electric dipolar resonances, and magnetic quadrupolar resonance. We changed the spectral positions of resonances by varying the DR heights, while keeping their diameters constant. Decreasing the heights of resonators allowed for moving both dipolar resonances to the blue edge of the spectra and for shifting the frequencies of MDRs closer to EDRs frequencies, up to their coincidence. Such a coincidence is often considered in the literature as a critical condition for obtaining full transmission through MSs with 2π phase control. In this work, we intended to get a deeper insight onto the phenomenon of scattering from silicon MSs. For comparison with S-parameter spectra, we obtained BS and FS spectra and far-field patterns characterizing radiation from MS fragments. In addition, to visualize spectral changes of BS and FS dependent on DR geometry, we simulated 3D patterns, in which color changes were used to represent variations of scattered power density.

We compared the characteristics of single spherical and cylindrical DRs, to identify in the latter the resonances analogous to dipolar and quadrupolar Mie resonances in spheres. It was found that, for sparsely packed MSs (with a lattice constant of 450 nm), coincidence of dipolar resonances did not provide dominant FS or full transmission of incident waves. Analysis of S-parameter spectra and BS/FS spectra allowed for detecting the realization of the 1st Kerker conditions in the range $f < f_{MDR}$ at decreasing DR heights. In addition, an opportunity was found for realizing similar conditions at $f > f_{EDR}$. The drops in BS spectra were found entirely corresponding to the drops in S11 spectra that allowed for suggesting that they were both controlled by the impedance specifics. The studies of densely packed MSs (with a lattice constant of 300 nm) revealed no effects characteristic for realizing Kerker's conditions of the 1st type at $f > f_{EDR}$. Instead, at DR heights below 160 nm, the S-parameter spectra of dense MSs demonstrated full transmission and no reflection at $f = f_{EDR}$. Responses of such type are not typical for conventional resonances. They could be explained by interference phenomena providing a kind of electromagnetically induced transparency in dense MSs. Analysis of field patterns in cross

Published under license by AIP Publishing.

sections of dense MSs allowed for relating the observed transparency to the specifics of field distributions in dense arrays, which could be interpreted as the sets of alternating dipoles.

Thus, although the possibility to observe a full transmission through dense MSs has been confirmed, it did not look related to combined two π-value jumps in phase at EDR and MDR. Coincidence of dipolar resonances was not found to be productive for directional scattering. In particular, full transmission at $f = f_{EDR}$ could be obtained at distant positions of two dipolar resonances in spectra. Our data show that better directivity could be realized at $f < f_{MDR}$ at the 1st Kerker conditions. Confirmation of realizing Kerker's effects in MSs composed of cylindrical silicon DRs with heights in the range from 240 down to 100 nm presents a valuable result of these studies. In addition, we have concluded that DRs in dense MSs do not respond as independent "meta-atoms" and that their responses become defined by integrated resonance fields.

ACKNOWLEDGMENTS

This work was supported by the National Science Foundation (NSF) under Award No. ECCS-1709991.

REFERENCES

[1]I. Staude, A. E. Miroshnichenko, M. Decker, N. T. Fofang, S. Liu, E. Gonzales, J. Dominguez, T. S. Luk, D. N. Neshev, I. Brener, and Y. Kivshar, "Tailoring directional scattering through magnetic and electric resonances in subwavelength silicon nanodisks," ACS Nano **7**(9), 7824–7832 (2013).

[2]B. S. Luk'yanchuk, N. V. Voshchinnikov, R. Paniagua-Domínguez, and A. I. Kuznetsov, "Optimum forward light scattering by spherical and spheroidal dielectric nanoparticles with high refractive index," ACS Photonics **2**, 993–995 (2015).

[3]Y. F. Yu, A. Y. Zhu, R. Paniagua-Domınguez, Y. H. Fu, B. Luk'yanchuk, and A. I. Kuznetsov, "High-transmission dielectric metasurface with 2π phase control at visible wavelengths," Laser Photonics Rev. **9**(4), 412–418 (2015).

[4]A. I. Kuznetsov, A. E. Miroshnichenko, M. L. Brongersma, Y. S. Kivshar, and B. Luk'yanchuk, "Optically resonant dielectric nanostructures," Science **354**, 6314 (2016).

[5]M. Kerker, D.-S. Wang, and C. L. Giles, "Electromagnetic scattering by magnetic spheres," J. Opt. Soc. Am. **73**, 765–767 (1983).

[6]W. Liu and Y. S. Kivshar, "Generalized Kerker effects in nanophotonics and meta-optics," Opt. Express **26**(10), 13085–13105 (2018).

[7]J. M. Geffrin, B. García-Cámara, R. Gómez-Medina, P. Albella, L. S. Froufe-Pérez, C. Eyraud, A. Litman, R. Vaillon, F. González, M. Nieto-Vesperinas, J. J. Sáenz, and F. Moreno, "Magnetic and electric coherence in forward- and back-scattered electromagnetic waves by a single dielectric subwavelength sphere," Nat. Commun. **3**, 1171 (2012).

[8]S. Person, M. Jain, Z. Lapin, J. J. Sáenz, G. Wicks, and L. Novotny, "Demonstration of zero optical backscattering from single nanoparticles," Nano Lett. **13**, 1806–1809 (2013).

[9]Y. H. Fu, A. I. Kuznetsov, A. E. Miroshnichenko, Y. F. Yu, and B. Luk'yanchuk, "Directional visible light scattering by silicon nanoparticles," Nat. Commun. **4**, 1527 (2013).

[10]M. I. Tribelsky, J.-M. Geffrin, A. Litman, C. Eyraud, and F. Moreno, "Small dielectric spheres with high refractive index as new multifunctional elements for optical devices," Sci. Rep. **5**, 12288 (2015).

[11]Z. Wang, N. An, F. Shen, H. Zhou, Y. Sun, Z. Jiang, Y. Han, Y. Li, and Z. Guo, "Enhanced forward scattering of ellipsoidal dielectric nanoparticles," Nanoscale Res. Lett. **12**(1), 58 (2017).

[12]E. Semouchkina, G. B. Semouchkin, M. Lanagan, and C. A. Randall, "FDTD study of resonance processes in metamaterials," IEEE Trans. Microw. Theory Tech. **53**(4), 1477–1487 (2005).

[13]M. S. Wheeler, J. S. Aitchison, and M. Mojahedi, "Coupled magnetic dipole resonances in sub-wavelength dielectric particle clusters," J. Opt. Soc. Am. B **27**, 1083 (2010).

[14]N. Liu and H. Giessen, "Coupling effects in optical metamaterials," Angew. Chem. Int. Ed. Engl. **49**, 9838 (2010).

[15]F. Zhang, L. Kang, Q. Zhao, J. Zhou, and D. Lippens, "Magnetic and electric coupling effects of dielectric metamaterial," New J. Phys. **14**, 033031 (2012).

[16]N. Gandji, G. Semouchkin, and E. Semouchkina, "Electromagnetic responses from planar arrays of dielectric nano-disks at overlapping dipolar resonances," in *IEEE Conference on Research and Applications of Photonics in Defense (RAPID)* (IEEE, 2018).

[17]I. Staude and J. Schilling, "Metamaterial-inspired silicon nanophotonics," Nat. Photonics **11**, 274–284 (2017).

[18]E. Semouchkina, "Resonance field analysis and electromagnetic coupling effects in metamaterials structures," in *Metamaterials Classes, Properties and Applications* (Nova Science Publishers, 2011), pp. 137–164, ISBN 978-1-61668-958-2

Published under license by AIP Publishing.